

# MEASUREMENT OF SRT DISH PRIMARY BEAM PROFILE

**JAMIE RIGGS**

*Deep Space Exploration Society, 5921 Niwot Road, Longmont, CO 80503, USA.*

Email: jamiedses@spannedsolutions.com

---

A project to characterize the beam profile of the primary lobe of a 2.3-meter, parabolic dish, using a quarter-wave dipole connected to a receiver system centered at 1.42GHz embedded within a feed horn at the dish focus, was conducted at the Front Range Community College, Boulder County, Colorado. Antenna theory provides sufficient information to design an experiment to provide the beam profile, using the Sun as a source, in two orthogonal dimensions. A central composite experimental design is used to generate a second order, rotatable, response surface of antenna temperature versus the two spatial dimensions. The date and time of day are treated as a covariate variable as the azimuth and elevation dish mount permits an orthogonal dish beam projection onto the celestial sphere only when the Sun's center is the coordinate system origin at the local meridian. The primary lobe profile is elliptical in which the maximum (stationary point) is shifted from the solar-based coordinate origin by  $(1.23^\circ, -0.15^\circ)$ . The Half-Power Beam Width is  $14^\circ$  in azimuth and  $12^\circ$  in elevation. This two-dimensional temperature response surface, central composite experimental design is a method not currently used for determining beam profiles, and, as the number of sample points is optimized for a preselected power of test, gives the minimum samples needed.

---

## 1. INTRODUCTION

Radio sources with apparent positions on the Celestial Sphere radiate energy which may be collected and focused by the Front Range Community College (FRCC) 2.3-meter dish for reception by an antenna in the feed (Illustration 1). This system does not have the capability of forming an image; rather we can interpret each observation as a single pixel whose dimensions are herein to be determined.

The Massachusetts Institute of Technology (MIT) Haystack Observatory (2009) has developed a Small Radio Telescope (SRT) capable of continuum and spectral line observations in the L-band (1.42GHz). This inexpensive radio astronomy kit is intended to introduce students and amateur astronomers to the field of radio astronomy. The SRT is designed as a teaching tool, as it involves the combined technologies of microwave engineering and digital computing. It involves astronomy, digital signal processing, software development, and data analysis.

The SRT is a standard 2.3-meter diameter satellite television dish mounted on top of a motorized Az-El mount. This mount allows the observer to perform total power measurements and contour mapping. Software has been provided for controlling the antenna and selection of sources. Data reduction can be performed using existing radio astronomy software packages or other analysis systems preferred by the observer.

The single pixel data captured from the SRT is used to determine the geometry of the projected beam onto the Celestial Sphere. This geometry includes both the area and the profile of the projection. The beam pattern discerned from the geometry is characterized by beamwidth defined as the solid angle measure at the half-power level of the main lobe. The half-power beamwidth, known as the Full-Width Half Maximum (FWHM), can be measured from

observations deliberately chosen on coordinate axes centered on a bright celestial radio source such as the Sun.



*Illustration 1: FRCC SRT during installation and alignment.*

### 1.1 Problem Statement

The beam profile, measured as antenna temperature in degrees Kelvin, for the 2.3-meter dish is unknown. To analyze the coupling of the radio telescope to a celestial

source, the beam pattern and the aperture efficiency are required. The beam profile and beam solid angle are relevant, particularly for point sources, to understand confusion from sources not of interest but that may be present in the beam pattern.

### 1.2 Objectives

- Measure the beamwidth as projected in azimuth.
- Measure the beamwidth as projected in elevation.
- Determine the beam profile.
- Compare the beamwidths with the theoretical parabolic dish beamwidth and diffraction limit.

### 1.3 Background

COSMOS is a senior project group at the University of Colorado at Boulder. The primary goal of the COSMOS project is to design, fabricate, and implement a feedback control system for a high gain antenna capable of tracking celestial objects and satellites in earth orbit. This effort requires an antenna pattern characterization for an 18-meter dish, orbital and celestial coordinate determination software, and mechanical analysis. Professors, DSES, the Institute for Telecommunication Sciences (ITS), the Air Force, and other groups can use the dish for their own studies. This 2.3m dish study for the FRCC SRT is considered a pilot run for the 18m dish beam profile study.

## 2. EXPERIMENT DESIGN

We wish characterize the beam profile in two orthogonal directions measured by astronomers on the celestial sphere as Right Ascension ( $\alpha$ , in units of hours, minutes, and seconds), which is parallel to the direction of the Earth's rotation, and Declination ( $\delta$ , measured in degrees), which is measured orthogonally to the direction of the Earth's rotation. The instantaneous projection of the 2.3m dish beam onto the celestial sphere is not expected to be the intuitive circle.

This experiment utilizes a celestial source (Sun, Cas A, etc.) and a preselected frequency (1.42GHz, 1.665GHz, etc.) to determine the beam profile. This document will concern itself with the Sun as the celestial source, and 1.42GHz receiving frequency (HI). Illustration 2 shows the apparent solar diameter at various wavelengths (Kraus, 1986).

The factors that can be manipulated are time of day and season of the year (i.e., position of the celestial source), and the beam projected position relative to the Sun. This experiment fixes the integration time per sky location a 1 minute (115 0.52sec integrations) which demands reliable tracking for that period, and the positions at which the integration occurs. Hence, the only controlled factor is the position of the beam relative to the Sun. The response variable is the temperature in degrees Kelvin measured at the receiver. An idealized representation of the relative, non-normalized power is shown in Illustrations 3 and 4. The axes

are  $\alpha$  in degrees,  $\delta$  in degrees, and relative power, P. The actual beam profile will be determined from the experimental data.

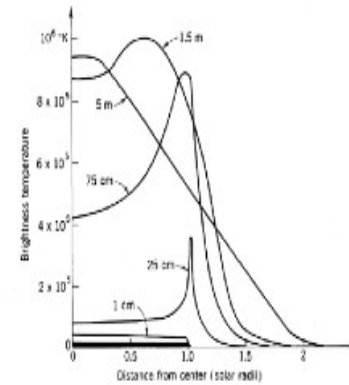


Fig. 7-5 Appearance of the radio sun on different wavelengths of observation. The visible sun is indicated by the heavy line.

Illustration 2: Appearance of the radio Sun on different wavelengths (Kraus, 1986).

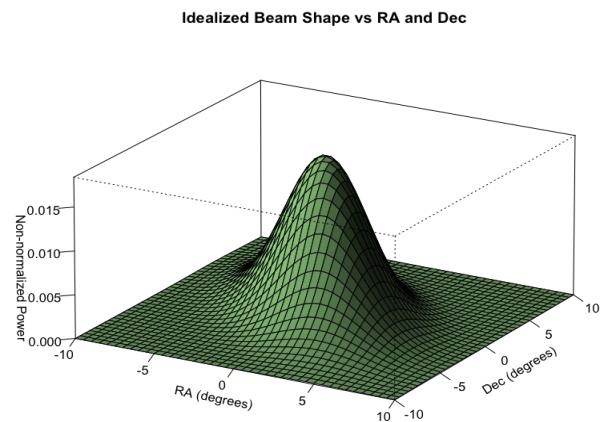


Illustration 3: Idealized beam profile wireframe plot.

The paths used in this experiment are displayed in Illustration 5. The dish motion is in 2 directions across 4 paths. The path labels are  $\alpha$  for Right Ascension,  $\delta$  for Declination, and  $\alpha\delta 1$  and  $\alpha\delta 2$  for the interaction between  $\alpha$  and  $\delta$ . These 4 paths will account for beam profile asymmetry between the two dimensions. Notice that the each axis has an orthogonal component. This assures the independence of the observations, and with the judicious choice of observations on these axes, nonlinear effects may be identified.

An efficient class of experimental designs for fitting second-order response surface models is well developed. Response surface methods are a collection of experimental strategies, mathematical methods, and statistical inference,

which, when combined, permit efficient and detailed exploration of cause and effect systems. We are interested in finding a suitable approximating function for predicting future response, and determining what values of the position values that maximize the response.

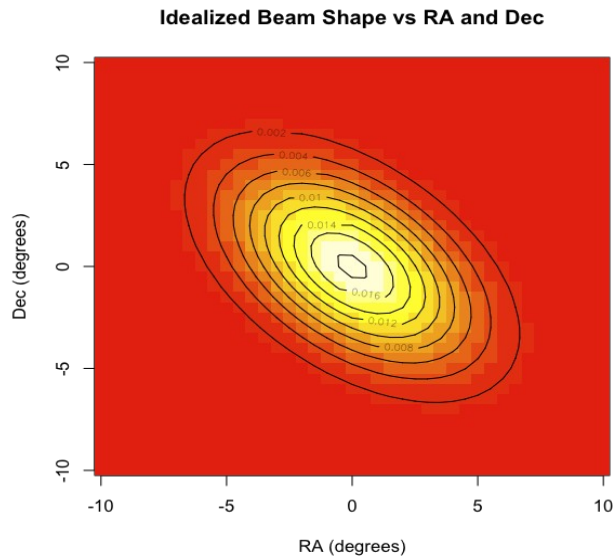


Illustration 4: Idealized beam profile contour plot.

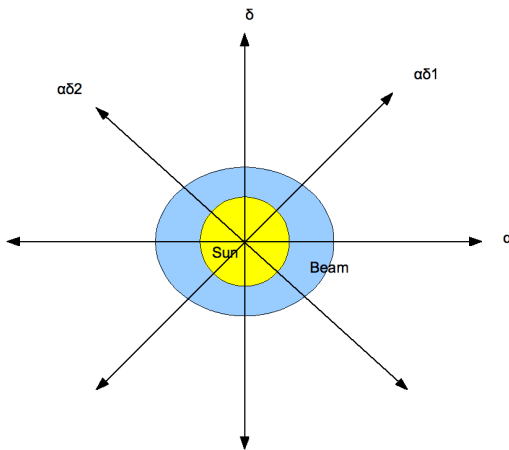


Illustration 5: Representation of the Solar disk (yellow) covered by the 18m dish beam (blue) projected onto the celestial sphere.

Although the eventual goal in the response surface analysis is to answer certain questions about the coupling characteristics of the 2.3m dish beam, it is extremely important that at the outset the decision be made regarding what beam positions relative to the Solar position are desired. These are known as central composite designs. Antenna theory and experimental evidence have given clear expectations of the beam characteristics. This allows us to

concisely choose the Sun-relative positions necessary for a thorough characterization of the 2.3m dish beam pattern.

An important property in our study design is rotatability. A design is said to be rotatable when the variance of the estimated response, which depends on the position particularly as it relates to the date and time, is a function only of the distance from the center of the design; viz., the center of the Sun; and not on the direction from this center. Thus, a rotatable design is one for which the temperature estimate is the same for two points that are the same distance from the design center.

Illustration 6 depicts 7 beam positions relative to the Sun center along the  $\alpha$  axis. The beam centers differ by  $1^\circ$ . Two additional positions along the  $\alpha$  axis approximately  $8^\circ$  to either side of the Solar limb are needed to establish baseline background power levels. Illustrations 7 and 8 show similar beam center positions along the  $\delta$  and the two  $\alpha\delta$  axes. These positions satisfy the two major requirements of rotatability, and the necessity for sufficient detection of temperature level changes.

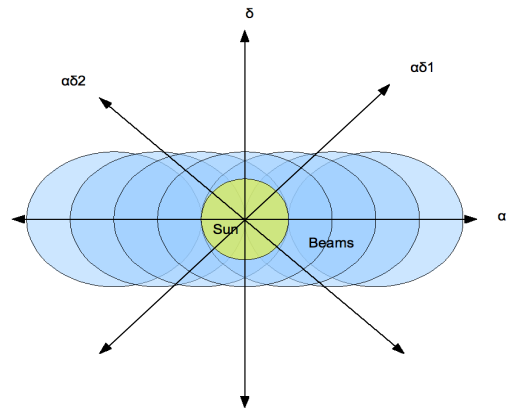


Illustration 6: Beam positions along the  $\alpha$  axis.

## 2.1 Model

The central composite design for fitting a second order response surface must involve at least three levels of each of the  $\alpha$  and  $\delta$  coordinates so that the coefficients in the model can be estimated. Response surface techniques depend on the method of least squares, specifically multiple regression. The actual form of the temperature response can be approximated by a polynomial function of second order:

$$y_i = \beta_0 + \beta_1 \alpha_i + \beta_2 \delta_i + \beta_{11} \alpha_i^2 + \beta_{22} \delta_i^2 + \beta_{12} \alpha_i \delta_i + \epsilon_i, \quad i = 1, 2, \dots, n,$$

where  $\beta_0$ ,  $\beta_1$ ,  $\beta_2$ ,  $\beta_{11}$ ,  $\beta_{22}$ , and  $\beta_{12}$  are constant coefficients,  $y_i$  is the measured response, and  $\epsilon_i$  is a random error used primarily to account for the inability to describe the true model, and  $i$  indicates the

experimental run number. We assume  $\epsilon_i \sim \text{iid } n(0, \sigma^2)$ , where  $\sim \text{iid } n(0, \sigma^2)$  is read as "distributed as identically independent normal with mean 0 and variance  $\sigma^2$ ".

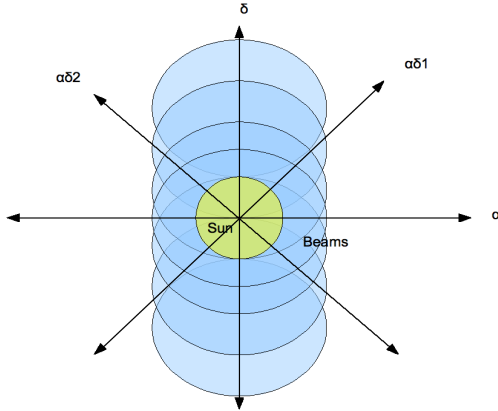


Illustration 7: Beam positions along the  $\delta$  axis.

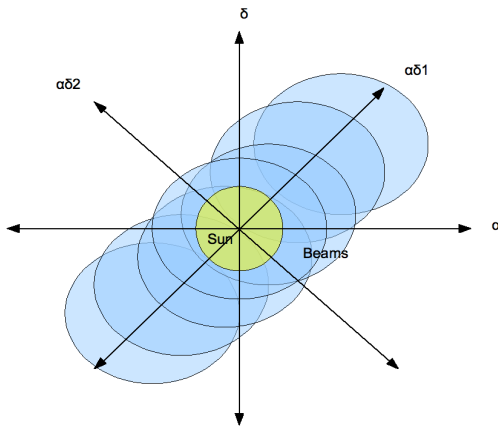


Illustration 8: Beam positions along the  $\alpha\delta 1$  axis.

The least squares estimates of the coefficients will be biased estimates in the presence of asymmetry unless we standardize the levels of  $\alpha$  and  $\delta$ . The procedure is

$$\alpha_i^* = \frac{(\alpha_i - \bar{\alpha})}{\sigma_\alpha} \text{ and } \delta_i^* = \frac{(\delta_i - \bar{\delta})}{\sigma_\delta},$$

where  $\bar{\alpha}$  and  $\bar{\delta}$  are the means of the coordinate observations, and  $\sigma_\alpha$  and  $\sigma_\delta$  are the respective coordinate observation standard deviations. Our coordinates are chosen to assure observations are from orthogonal and rotatable positions. This assures symmetry, and hence, coding is not necessary for unbiased model parameter estimates.

## 2.2 Sample Size

The method for determining the number of replications of coordinate combinations is based on a test of a hypothesis about differences among coordinate group means with known variance  $\sigma^2$ , using the standard normal distribution test statistic. The method determines the sample means with specified Type I and Type II errors. A Type I error is a false positive error, and a Type II error is a false negative error.

To remain consistent with statistical convention, for this section only, we redefine  $\alpha$ ,  $\beta$ , and  $\delta$ . All other sections use these variables as defined in the previous sections.

The required number of replications is affected primarily by four factors that are required for calculations: The variance,  $\sigma^2$ ; the size of the difference that has physical significance between two means,  $\delta$ ; the significance level of the test,  $\alpha$ , which is the probability of Type I error; the power of test  $1-\beta$ , which is the probability of detecting  $\delta$ , where  $\beta$  is the probability of a Type II error.

The required replication number  $n$ , for each coordinate, for two-sided alternatives is estimated with

$$n \geq 2 \left[ z_{\alpha/2} + z_\beta \right]^2 \left( \frac{\sigma}{\delta} \right)^2,$$

where  $z_{\alpha/2}$  is the standard normal variate that must be exceeded with probability  $\alpha/2$  to indicate significance, and  $z_\beta$  variate that must be exceeded with probability  $\beta$  to indicate significance.

Assume  $\alpha=0.05$ ,  $\beta=0.1$ ,  $\sigma=0.5^\circ$ , and  $\delta=1^\circ$ . Then  $z_{\alpha/2}=1.96$  and  $z_\beta=0.04$ , which give a power of a test of 90%, and we have

$$n \geq 2 \left[ z_{\alpha/2} + z_\beta \right]^2 \left( \frac{\sigma}{\delta} \right)^2 = 2(1.96 + 0.04)^2 \left( \frac{0.5}{1.0} \right)^2 = 2.$$

Therefore, each beam center location temperature measurement relative to the Sun's location is repeated 2 times. There are 4 axes along which 8 locations are measured 2 times in increments of  $1^\circ$  from the Sun's center, the 4 axes have 2 background noise locations repeated 2 times with the beam center at least  $8^\circ$  from Sol center, and 1 location at Sol center measured 2 times. This gives the total number of observations,  $N$ , as

$$N = 4 \times 8 \times 2 + 4 \times 2 \times 2 + 2 = 82.$$

If we assume an average of 1 minute between successive observations, and an integration time of 1 minute, the the total time to complete the measurements will range between 2 and 3 hours. A reasonable run time is from 10:30 A.M. to 1:30 P.M. local time. The measurements then will be taken just before and after the Sun crosses the local

meridian.

If all 82 measurements cannot be taken in a single session, the experiment can be blocked to divide the 82 measurements in two or more sessions. Blocking removes degrees of freedom from parameter estimation, but tends to homogenize the variance within blocks.

### 2.3 Randomization

An argument can be made to say that the single most significant contribution of mathematical statistical science to the natural and engineering sciences collectively is introducing randomization into the experimental process. Laboratory experimentation attempts, usually quite successfully, to control all the factors suspected or known to affect the outcome of an experiment. However, even with stringent factor control, variability still manifests with unequal repeated observations.

Statistical analysis of data from experiments assumes the observations constitute a random sample from, often, a normally distributed population. This assumption is plausible for comparative observational studies that use random samples of the available observation units from different values.

Independent observations are critical for unbiased estimation and tests of hypotheses as they provide valid estimates of experimental error variance. However, the assumption of independence among the experimental units cannot be justified when relationships exist between them as a result of not randomizing observation order. Thus, the necessity for randomizing the order of the measurement locations used in this study.

## 3. ANALYSIS

We first examine the descriptive properties of the temperature versus location data. This includes distribution histograms, scatter plots, and box plots. With this information, we examine the parametric relationship between the temperature and location, thus providing a predictive aspect.

### 3.1 Descriptive Analysis

We examine the antenna temperature against the azimuth locations, and then against elevation locations. The data show that the shapes might be estimated by a normal distribution (Illustrations 9 and 10). However, closer examination of these data reveal a disturbing aspect of the range of temperature at Sol center: the temperature ranges from 2,104°K) to 10,979°K. The expected values are temperatures that would vary by a few hundred degrees from the maximum. At least two possibilities for the anomalous data were investigated to understand the behavior of the data at Sol center. One possibility was receiver saturation, and the other was insufficient dwell time. Examination of the raw data clearly shows short dwell times on the majority of Sol

observations. The observations that were a full 1 minute duration indicate no saturation. However, it is advised that the receiver characteristics be reviewed to ascertain the potential for saturation with a source as strong as the Sun.

Temperature vs. Azimuth Displacement

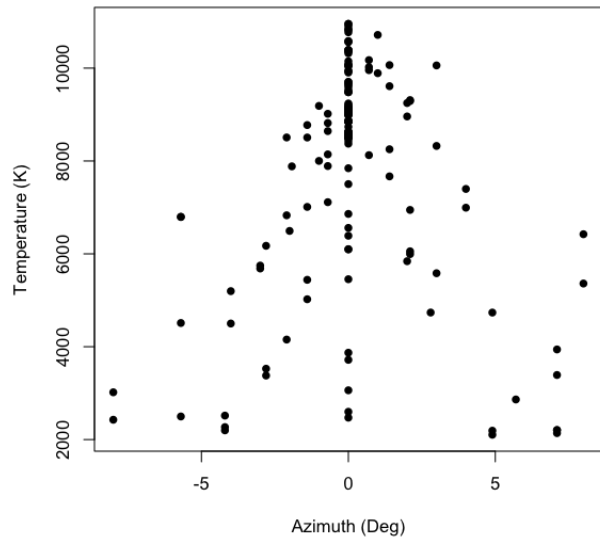


Illustration 9: Scatter plot of Temperature vs. Azimuth with 1 minute dwell data data appended.

Temperature vs. Elevation Displacement

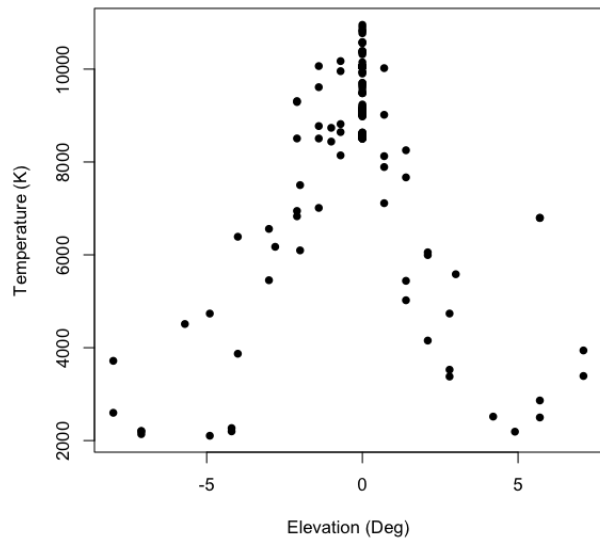


Illustration 10: Scatter plot of Temperature vs. Elevation with 1 minute dwell data data appended.

The short dwell time conjecture was tested by taking additional Sol center measurements. These additional observations were appended to the original data set after first eliminating all the short dwell time, Sol center observations.

As seen in Illustrations 9 and 10, the data set now appears as expected. Note that the lower temperatures at Sol center are from locations along the elevation axis in the Azimuth scatter plot, and from location along the azimuth axis in the Elevation scatter plot.

As multiple observations were made at each point in the azimuth and elevation plane, the scatter plots are also presented with box plots at each value of azimuth and elevation (Illustrations 11 and 12). Notice that for the most part, the box plots are symmetric about their respective medians. This is desirable for response surface analysis.

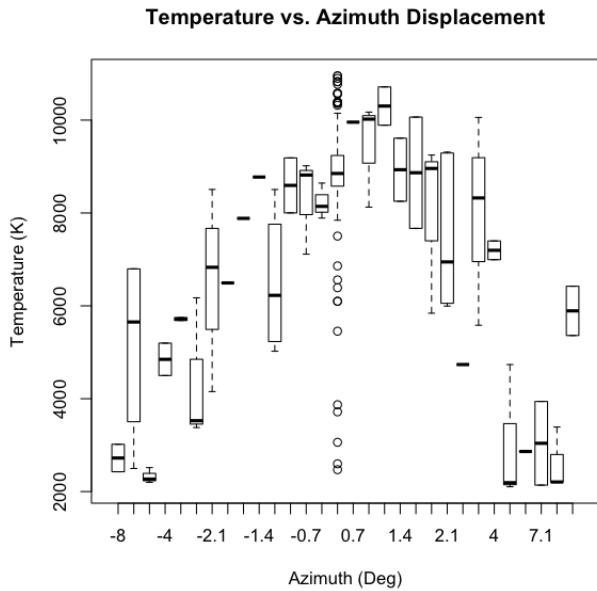


Illustration 11: Box plots of Temperature vs. Azimuth. The lower outlier values at Sol center are from non-zero elevation locations.

Illustration 13 is a histogram of the temperature distribution. The asymmetry of the histogram at Sol center is due to collapsing two dimensions into one.

### 3.2 Response Surface Analysis

Response-surface methodology comprises a suite of methods for exploring for optimum operating conditions through experimental methods. Often, this involves running several experiments, using the results of one experiment to provide direction for what to do in the next. This next action could be to focus an experiment with different sets of conditions, or to collect more data in the current experimental region in order to fit a higher-order model, or to confirm existing findings.

Multiple levels of the operating conditions are what constitute the factors in each experiment. Our experiment involves the measured antenna temperatures resulting from positioning the SRT dish at predetermined offsets from the Solar center. The fundamental methods for quantitative variables involve a fit of either first-order (linear) or second-order (quadratic)

functions of the predictor coordinates to the response variable temperature, and then examining the characteristics of the fitted surface to decide what action is appropriate.

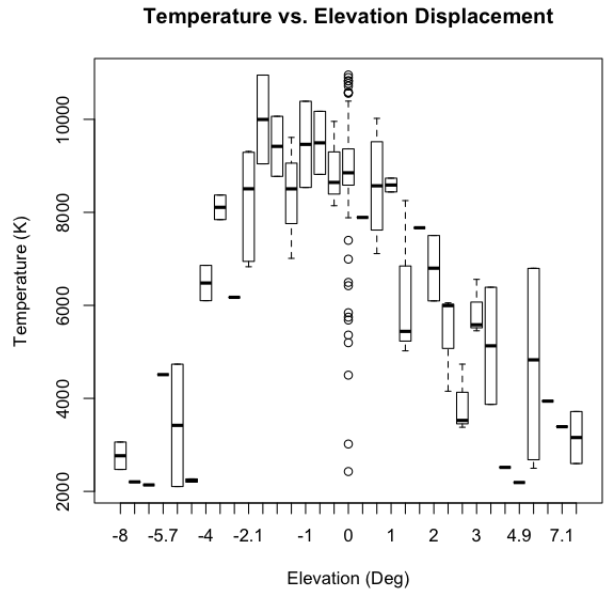


Illustration 12: Box plots of Temperature vs. Elevation. The high temperatures on the negative side of zero may be due to non-primary lobes interacting with roof tops. The lower outlier values at Sol center result from collapsing two dimensions into one..

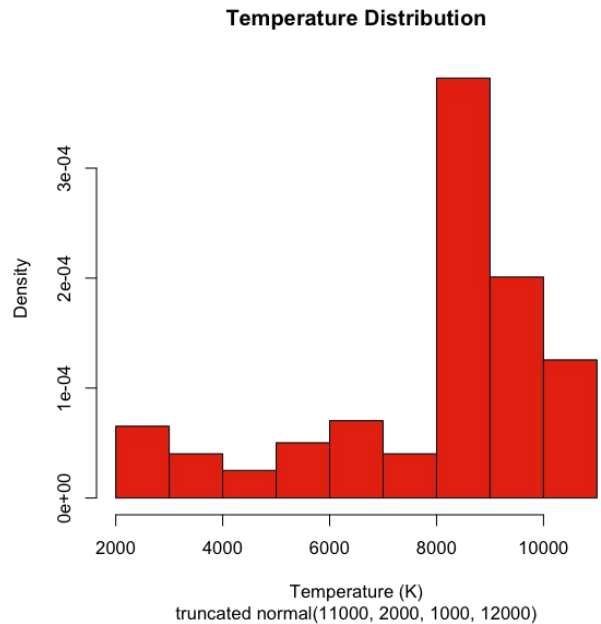


Illustration 13: Histogram of Temperature with both axes collapsed into a single dimension. The asymmetry is due to a predominance of observation near Sol center.

Given this sequence of actions, it may seem like response-surface analysis can be reduced to a regression

problem. However, there are several intricacies in this analysis as well as how it is commonly used that differ enough from routine regression problems that some special attention is warranted. These intricacies include the common use (and importance) of coded predictor variables; the assessment of the fit; the follow-up analyses that are used depending on what type of model fits the data, as well as the outcome of the analysis; and the importance of visualizing the response. Response-surface methods also involve some unique experimental-design issues, due to the emphasis on iterative experimentation and the need for relatively sparse designs that can be built-up piece-by-piece according to the evolving needs of the experimenter.

The analysis-of-variance table for response surface analysis includes a breakdown of lack of fit and pure error, as well as information about the direction of steepest ascent (Myers, 1976). The steepest-ascent information must be used with caution as there is significant lack of fit for this model ( $p < 0.01$ ). It suggests that we should try a higher-order model, or collect additional data. The experiment design uses data that are from a full central-composite design, so lack of fit may be improved by increasing the number of repeated values from the existing coordinate locations (Box and Draper, 1987). This will repair any marginal temperature by location values so fewer inflection points will result. An alternative is to collect additional data off the axes but at the radii already used. The use of additional data is relegated to another experiment, and hence is not discussed here.

The summary for the second-order model, presented below, provides results of a canonical analysis of the surface rather than for steepest ascent. The analysis indicates that the stationary point of the fitted surface is at  $(1.23^\circ, -0.15^\circ)$  which is well within the experimental region; and that both eigenvalues are negative, indicating that the stationary point is a maximum (Box and Draper, 2007). This is clear evidence of a nearby set of optimal conditions. Optionally, additional data may be collected in the vicinity of the stationary point to confirm or correct this location.

```
Call:
rsm(formula = y ~ S0(x1, x2), data = X)

Residuals:
    Min       1Q   Median       3Q      Max
-4000.56 -677.53  -33.97  1178.53  4474.63

Coefficients:
              Estimate Std. Error t value Pr(>|t|)
(Intercept)  9195.704    122.318   75.179 < 2e-16 ***
x1           198.041     51.109    3.875 0.000146 ***
x2          -20.057     51.822   -0.387 0.699164
x1:x2        -8.499     11.451   -0.742 0.458863
x1^2         -80.864      9.799   -8.252 2.39e-14 ***
x2^2        -100.890      9.792  -10.303 < 2e-16 ***
---
Signif. codes:  0 '***' 0.001 '**' 0.01 '*' 0.05 '.' 0.1 ' ' 1

Residual standard error: 1566 on 193 degrees of freedom
Multiple R-squared:  0.6186,    Adjusted R-squared:  0.6087
F-statistic: 62.61 on 5 and 193 DF,  p-value: < 2.2e-16

Analysis of Variance Table

Response: y
          Df Sum Sq Mean Sq F value Pr(>F)
FO(x1, x2) 2  3813451  1906725  0.7776 0.46096
TWI(x1, x2) 1  12841941  12841941  5.2369 0.02320
```

```
PQ(x1, x2)    2 751007352 375503676 153.1299 < 2e-16
Residuals    193 473272761 2452190
Lack of fit   41 319531571 7793453 7.7052 < 2e-16
Pure error    152 153741190 1011455
```

```
Stationary point of response surface:
      x1      x2
1.2324883 -0.1513096
```

```
Eigenanalysis:
$values
[1] -79.99921 -101.75404

$vectors
      [,1] [,2]
[1,] -0.9799323 0.1993304
[2,]  0.1993304 0.9799323
```

While the canonical analysis gives us a description on the behavior of a second-order response surface, a graph of the response surface is revealing. Illustrations 14 and 15 include both a heat map and contour levels of the fitted response surface. The response in Illustration 14 is Temperature in degrees Kelvin, and the response in Illustration 15 is power in milliwatts. The fitted response surface is obtained from the second order equation given in the ANOVA summary above:

$$y = 9195.7 + 198.0x_1 - 20.1x_2 - 8.5x_1x_2 - 80.9x_1^2 - 100.9x_2^2.$$

The plot displays a color image overlaid by the contour lines. It is clear that the SRT beam profile is elliptical, with the elevation ( $x_2$ ) axis as the minor axis of the ellipse. Also, it is quite clear that the stationary point is not located at  $(0,0)$  as one would expect. We suspect this is due to misalignment of the feed horn from the dish central axis which, during installation of the dish, it was determined from the solar shadow projected onto the dish center, that a 1 degree offset in azimuth was needed to place the feed horn on the dish axis. Rerunning this experiment with this offset removed may result in the stationary point lying closer to  $(0,0)$ .

We emphasize that, although the fitted values are also displayed (the contour ellipses), we must be aware that these are model predictions and that, as the distance from the plot center increases, the prediction error increases. Additional experimental runs at selected points, and use the observed response values, not the predictions, may be used for guidance on where to locate a next experiment.

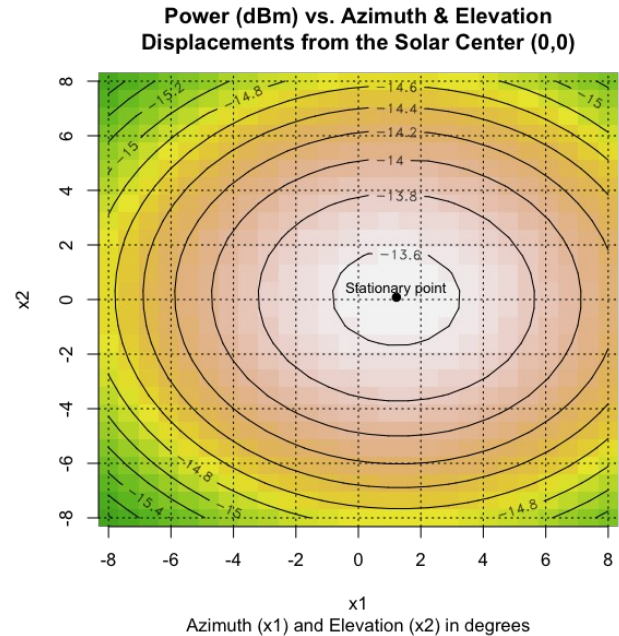
In the second-order case, the steepest ascent function works, but it uses the ridge analysis method (Draper 1963), which is the analog of steepest ascent in the sense that, for a specified distance  $r$ , it finds the point at which the predicted response is a maximum among all predictor combinations at radius  $r$ . This method makes sense when the stationary point is some distance away from the steepest function; but when this point is nearby, it makes more sense to start at the saddle point (rather than the origin, if it exists) and follow the most steeply rising ridge in both directions. This path is obtained using a canonical path function. In this function, distance is a signed quantity, according to the direction along the ridge.

In our study, we have a nearby stationary point. Here are some points within a radius of  $5^\circ$  along the canonical

path:

	dist	x1	x2	yhat
1	-5.0	6.132	-1.148	7319.394
2	-4.5	5.642	-1.048	7699.451
3	-4.0	5.152	-0.949	8039.365
4	-3.5	4.662	-0.849	8339.407
5	-3.0	4.172	-0.749	8599.433
6	-2.5	3.682	-0.650	8819.364
7	-2.0	3.192	-0.550	8999.375
8	-1.5	2.702	-0.450	9139.371
9	-1.0	2.212	-0.351	9239.319
10	-0.5	1.722	-0.251	9299.299
11	0.0	1.232	-0.151	9319.263
12	0.5	0.743	-0.052	9299.307
13	1.0	0.253	0.048	9239.334
14	1.5	-0.237	0.148	9139.346
15	2.0	-0.727	0.247	8999.407
16	2.5	-1.217	0.347	8819.404
17	3.0	-1.707	0.447	8599.385
18	3.5	-2.197	0.546	8339.462
19	4.0	-2.687	0.646	8039.429
20	4.5	-3.177	0.746	7699.379
21	5.0	-3.667	0.845	7319.474

elevation..



**Temperature (K) vs. Azimuth & Elevation Displacements from the Solar Center (0,0)**

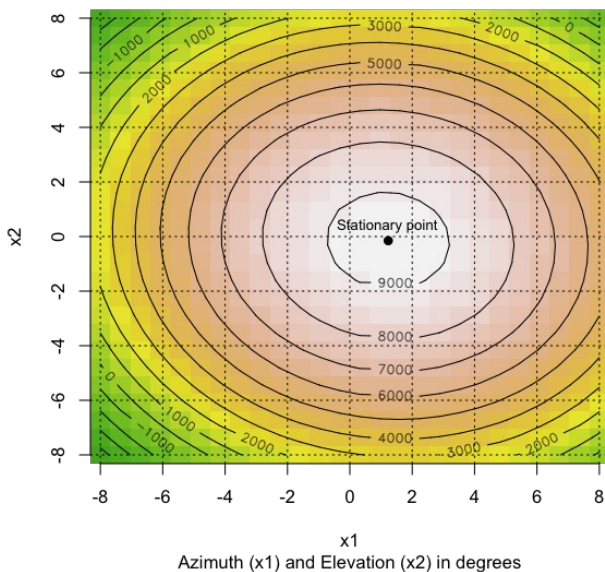


*Illustration 14: Contour plot of the beam profile. The stationary point is (1.23°, -0.15°).*

To determine the Half Power Beam Width (HPBW), we subtract the noise-level average temperature from the temperature at the stationary point, halve this difference, then subtract the halved difference from the temperature at the stationary point. From Illustration 15, we have

$$(9,312.9 + 868.8) / 2 = 5,090.8.$$

Locating the 5,000 contour ellipse intersections on both the azimuth and elevation axes, we have that the HPBW is approximately 14 degrees in azimuth and 12 degrees in

*Illustration 15: Contour plot of the beam profile. The stationary point is (1.23°, -0.15°).*

The theoretical HPBW for a parabolic dish is approximated by

$$HPBW = 70 \left( \frac{\lambda}{d} \right) = 70 \left( \frac{0.21m}{2.3m} \right) = 6.39^\circ,$$

where  $\lambda$  is the wavelength of signal of interest, and  $d$  is the diameter of the dish. Clearly, the empirical HPBW is approximately twice the theoretic al value. The estimated diffraction limit is approximated by

$$\theta = 1.22 \left( \frac{\lambda}{d} \right) = 1.22 \left( \frac{0.21m}{2.3m} \right) = 0.111.$$

#### 4. CONCLUSIONS

The Massachusetts Institute of Technology Haystack Observatory (2009) has developed a Small Radio Telescope (SRT) capable of continuum and spectral line observations in the L-band (1.42GHz). The beam profile, measured as antenna temperature in degrees Kelvin, for the 2.3-meter dish was unknown. To analyze the coupling of the radio telescope to a celestial source, the beam pattern and the aperture efficiency are required. The beam profile and beam solid angle are relevant, particularly for point sources, to understand confusion from sources not of interest but that may be present in the beam pattern. We measured the beamwidth as projected in azimuth and in elevation, and compared it to the SRT estimated diffraction limit.

We characterized the beam profile in two orthogonal directions measured by astronomers on the celestial sphere as Right Ascension ( $\alpha$ , in units of hours, minutes, and seconds), which is parallel to the direction of the Earth's rotation, and Declination ( $\delta$ , measured in degrees), which is measured orthogonally to the direction of the Earth's rotation.

This experiment utilizes a celestial source (Sun, Cas A, etc.) and a preselected frequency of 1.42GHz to determine the beam profile. The factors manipulated were time of day and season of the year (i.e., position of the celestial source), and the beam projected position relative to the Sun. This experiment fixes the integration time per sky location a 1 minute (115 0.52sec integrations) which demands reliable tracking for that period, and the positions at which the integration occurs. Hence, the only controlled factor is the position of the beam relative to the Sun. The response variable is the antenna temperature in degrees Kelvin measured at the receiver.

Response-surface methodology was used to analyze the central composite experimental design structure to form a quadratic antenna temperature response surface beam profile. This analysis shows the beam profile to be elliptical in with the major axis of the ellipse along the Right Ascension axis. The half power beam width in right ascension is 14 degrees, and the half power beam width in the declination direction is 12 degrees, which is approximately twice the theoretical value of 6.39 degrees. Rerunning this experiment is suggested using the alternative protocol described in Section 7. The alternative protocol may eliminate errors incurred from the manual coordinate entry used in this experiment.

The stationary point is  $(1.23^\circ, -0.15^\circ)$  off the Sol center. The estimated diffraction limit is 0.111. Each of these values derived from a sample size of 82, giving a power of test of 90%.

Using statistically designed experiments and response surface analysis methods, the minimum number of samples needed to satisfy a preset power of test provides confidence levels that hitherto are unreported in engineering beam profile determinations.

## 5. ACKNOWLEDGMENTS

John Minors provided access to the FRCC SRT. His continued presence greatly facilitated the production of this work.

Paul Berge gave his time to help operate and collect the data used in this study. Without his effort, the data collection process would have been very tedious.

Dennis Akos and John Ewan explained possible scenarios for why the Sol center data were skewed counter-intuitively. Their information significantly improved the analysis. Also,

their editorial comments are greatly appreciated.

## 6. REFERENCES

Box, G.E.P. and Draper, N.R., 1987, *Empirical Model-Building and Response Surfaces*, New York: John Wiley & Sons, Inc.

Box, G.E.P. and Draper, N.R., 2007, *Response Surfaces, Mixtures, and Ridge Analyses*, Hoboken, New Jersey: John Wiley & Sons, Inc.

MIT Haystack Observatory, 2009, <http://www.haystack.mit.edu/edu/undergrad/srt/index.html>

Kraus, J.D., 1986, *Radio Astronomy*, 2 ed., Durham, N.H.: Cygnus-Quasar Books, p. 8-47.

Myers, R.H., 1976, *Response Surface Methodology*, Virginia Polytechnic Institute and State University: Virginia.

## 7. PROTOCOL

The following protocol is the procedure to carry out the beam profile measurements. This protocol is designed to ensure the integrity of the assumptions required for unbiased statistical analyses. If a deviation from the protocol is necessary, the nature of the deviation must be thoroughly documented.

Prior to running the actual experiment, it is mandatory to run the first half-dozen to dozen runs, as indicated in the protocol, as a pilot. The pilot will help identify design difficulties and polish the experimenter's observing skill. If the pilot runs result in valid data, they need not be repeated when the experiment is run. In this case, the data collected from the pilot may be added to the data collected from the experiment, and used in the analysis.

1. Assure the 1.420GHz feed horn is properly mounted at the lower dish focal point and is functioning correctly.
2. Assure the back end receiving system is connected and operational.
3. Verify the data collection system generates and contains the correct data.
4. Move the suspected beam center at least  $2^\circ$  away from the next run location (see Section 8) in any direction after first selecting the Sun.
5. Move the suspected beam center to the run location and begin tracking.
6. Record the date and time.
7. Once tracking is stabilized, measure and record the power using a 1 minute integration time.
8. Cease recording and continue tracking for a few seconds.

9. Repeat steps 5 through 8 until all the planned experimental runs are complete.
10. Stow the dish.
11. Collect the data file or files for analysis.
12. Match the recorded power levels with the runs in Section 8. The data are now ready for statistical analysis. This includes subtracting the background power levels (locations 8° from Sol center) from the other power measurements, generating the antenna temperature beam profile, and testing for significant differences between the various power level contours.

An enhancement to the protocol is, as the SRT has azimuth and elevation travel limits that constrain the user to times when the Sun is close to local noon, is to use a maximum offset from the sun in order to establish a stable baseline for observations, and an off-source calibration position that will not be overpowered by the Sun. For the off-source calibration, an area at least two beamwidths (in azimuth, positive or negative) away from the sun is desirable. A sample command file for the central composite design listed in Section 8 is (MIT, 2009):

```

: record _BeamProfile /Start recording, output filename is
optional
: azel 130 45 /calibration position
: 1415.0 /center frequency with mode 1, 500MHz bw
(default)
: calibrate /calibration using vane calibrator
: noisecal /when using noise source (either vane OR noise)
: Sun /Source command
* Azimuth Scan /Comment
: offset -30 0 /start offset commands for scan -30 to +30
degrees
: offset -2.8 -2.8
: offset -1.4 1.4
: offset 1 1
: offset -2.8 2.8
: offset -25 0
etc. according to the table in Section 8
: roff /End recording

```

## 8. RANDOMIZED RUN SEQUENCE

Data at four additional locations (11.3° at ±ad1 and ±ad2) with two repetitions each for a total of eight were collected to assure a canonical coordinate system in the analysis.

Run	Radius	Theta	Axis	Run	Radius	Theta	Axis
1	4	225	-ad1	42	8	180	-a
2	2	135	+ad2	43	3	315	-ad2
3	1	45	+ad1	44	1	270	-d
4	4	135	+ad2	45	3	225	-ad1
5	3	45	+ad1	46	8	135	+ad2
6	2	315	-ad2	47	2	90	+d
7	3	135	+ad2	48	4	315	-ad2
8	4	180	-a	49	8	315	-ad2
9	8	90	+d	50	2	270	-d
10	8	45	+ad1	51	1	0	+a
11	4	90	+d	52	3	0	+a
12	1	315	-ad2	53	1	45	+ad1
13	1	0	+a	54	4	270	-d
14	8	180	-a	55	4	0	+a
15	1	90	+d	56	3	180	-a
16	4	135	+ad2	57	2	270	-d
17	3	315	-ad2	58	2	90	+d
18	8	90	+d	59	3	270	-d
19	2	225	-ad1	60	2	180	-a
20	1	90	+d	61	1	270	-d
21	3	0	+a	62	8	315	-ad2
22	8	135	+ad2	63	2	225	-ad1
23	2	45	+ad1	64	8	45	+ad1
24	2	180	-a	65	8	225	-ad1
25	4	45	+ad1	66	1	225	-ad1
26	3	45	+ad1	67	8	225	-ad1
27	0	0	0	68	1	180	-a
28	1	225	-ad1	69	2	0	+a
29	8	270	-d	70	2	315	-ad2
30	2	0	+a	71	1	315	-ad2
31	3	180	-a	72	3	135	+ad2
32	4	180	-a	73	1	180	-a
33	8	0	+a	74	3	270	-d
34	4	270	-d	75	4	0	+a
35	1	135	+ad2	76	4	225	-ad1
36	8	0	+a	77	3	90	+d
37	8	270	-d	78	4	90	+d
38	4	45	+ad1	79	2	45	+ad1
39	4	315	-ad2	80	2	135	+ad2
40	3	90	+d	81	1	135	+ad2
41	0	0	0	82	3	225	-ad1